J. Fluid Mech. (2013), *vol.* 718, *pp.* 596–621. © Cambridge University Press 2013
doi:10.1017/jfm.2012.626

Self-similar mean dynamics in turbulent wall flows

J. C. Klewicki†

Department of Mechanical Engineering, University of New Hampshire, Durham, NH 03824, USA
Department of Mechanical Engineering, University of Melbourne, Melbourne, VIC 3010, Australia

(Received 12 June 2012; revised 29 November 2012; accepted 12 December 2012;
first published online 8 February 2013)

This study investigates how and why dynamical self-similarities emerge with increasing Reynolds number within the canonical wall flows beyond the transitional regime. An overarching aim is to advance a mechanistically coherent description of turbulent wall-flow dynamics that is mathematically tractable and grounded in the mean dynamical equations. As revealed by the analysis of Fife, Klewicki & Wei (*J. Discrete Continuous Dyn. Syst.* A, vol. 24, 2009, pp. 781–807), the equations that respectively describe the mean dynamics of turbulent channel, pipe and boundary layer flows formally admit invariant forms. These expose an underlying self-similar structure. In all cases, two kinds of dynamical self-similarity are shown to exist on an internal domain that, for all Reynolds numbers, extends from $O(\nu/u_\tau)$ to $O(\delta)$, where ν is the kinematic viscosity, u_τ is the friction velocity and δ is the half-channel height, pipe radius, or boundary layer thickness. The simpler of the two self-similarities is operative on a large outer portion of the relevant domain. This self-similarity leads to an explicit analytical closure of the mean momentum equation. This self-similarity also underlies the emergence of a logarithmic mean velocity profile. A more complicated kind a self-similarity emerges asymptotically over a smaller domain closer to the wall. The simpler self-similarity allows the mean dynamical equation to be written as a closed system of nonlinear ordinary differential equations that, like the similarity solution for the laminar flat-plate boundary layer, can be numerically integrated. The resulting similarity solutions are demonstrated to exhibit nearly exact agreement with direct numerical simulations over the solution domain specified by the theory. At the Reynolds numbers investigated, the outer similarity solution is shown to be operative over a domain that encompasses $\sim$40 % of the overall width of the flow. Other properties predicted by the theory are also shown to be well supported by existing data.

Key words: turbulence theory, turbulent flows, turbulent boundary layers

1. Introduction

The purposes of this study are to demonstrate the existence of self-similar mean dynamics in turbulent wall flows, and to describe their emergence with increasing Reynolds number. Primary outcomes are the mathematical reasons underlying how, why and where within the flow the mean dynamical equations for the canonical

† Email address for correspondence: joe.klewicki@unh.edu

https://doi.org/10.1017/jfm.2012.626 Published online by Cambridge University Press

turbulent wall flows (pressure-driven flow in fully developed pipes and channels, and boundary layer flow over a flat plate) admit self-similar solutions.

Distinct from approaches that involve additional assumptions or hypotheses of a mathematical or phenomenological nature, the present theory is solely based upon the properties formally admitted by the leading-order representations of the relevant mean dynamical equations. The basis for exposing the self-similar structure is the same as that used to construct similarity solutions for laminar boundary value problems. To the author's knowledge, the existence of an authentic similarity solution for turbulent wall flows has not previously been demonstrated. Such solutions are inherently characterized by a coordinate stretching that accounts for the invariance of the properly normalized solution as the relevant parameter, in this case Reynolds number, varies. The coordinate stretching for turbulent wall flows is shown to be represented by the spatial variation of the size of the motions associated with the net mean effect of turbulent inertia. This has conceptual connection to von Kármán's mixing length similarity hypothesis (von Kármán 1930).

The relevant dynamical structure comes into being through the transitional regime. Prior to this regime, the dynamics of fully developed laminar Poiseuille flows is everywhere characterized by a balance between a driving pressure force and a retarding viscous force, while the dynamics of the laminar boundary layer is dictated by a retarding viscous force that effects a time rate of change of streamwise momentum. In each of these flows, instabilities emerge at sufficiently high Reynolds number, and the mechanism of turbulent inertia enters into the time-averaged statement of dynamics. The appearance of robust nonlinear interactions associated with turbulent inertia mark the onset of the transitional regime. These interactions lead to rapid rearrangements of the mean momentum distribution during the transitional regimes of channels, pipes and boundary layers (Elsnab *et al.* 2011; Klewicki, Ebner & Wu 2011; Klewicki *et al.* 2012). The transitional regimes culminate (albeit in each case by a different route) with the establishment of the four-layer regime first described by Wei *et al.* (2005).

The essential properties of the four-layer regime derive from the leading-order balance of terms in the mean momentum equation. This is briefly described in § 2.1. The persistence of the four-layer regime for all Reynolds numbers beyond the transitional regime is described in appendix A. This persistence is significant, since, with increasing Reynolds number, the scaling properties of the four-layer regime become increasingly well established (Fife *et al.* 2005*a*,*b*; Wei *et al.* 2005; Fife, Klewicki & Wei 2009; Klewicki, Fife & Wei 2009). Thus, the similarity structure described herein emerges with increasing Reynolds number. This situation is analogous to the similarity solution for the laminar boundary layer, as the accuracy of the laminar solution also improves with increasing Reynolds number. In each case this occurs because the terms that describe the leading-order dynamics become increasingly dominant.

Once in the four-layer regime, the mean dynamical equations admit invariant forms that determine the scaling behaviours of their solutions. The properties of these are described by the theory of Fife and coworkers (Wei *et al.* 2005; Fife *et al.* 2005*b*, 2009; Klewicki *et al.* 2009). An articulation of this theory sufficient to understand how and why the mean dynamical equations admit similarity solutions is presented in § 3, but without detailed derivation. These details are found in the previous publications cited. Sections 2 and 3 include descriptions of the scaling behaviours associated with the layer widths and their velocity increments, how and why the equations admit invariant forms interior to the boundaries of an internal

https://doi.org/10.1017/jfm.2012.626 Published online by Cambridge University Press

layer hierarchy, and a discussion of the factors influencing variations in the solution properties of the different canonical wall flows. Section 4 describes the functions that dictate the underlying similarity structure. These functions are physically related to the cross-stream flux of turbulent inertial force. Section 4 culminates with a demonstration of turbulent wall-flow similarity solutions. These solutions are found by numerically integrating the closed mean dynamical equations in a manner analogous to the procedure used to solve the Blasius boundary layer equation. Broader implications that derive from the existence of these similarity solutions, and self-similar mean dynamics in general, are discussed in the conclusions.

2. Fundamental properties of the mean force balance

We consider statistically stationary, fully developed, incompressible turbulent flow in pressure-driven pipes and planar channels, and in the developing zero-pressure-gradient boundary layer. The main flow is in the x direction, with the wall-normal direction denoted by y ($y = \delta - r$ in the pipe, where δ denotes the pipe radius). Upper-case letters or angle brackets denote time-averaged quantities; lower-case letters indicate fluctuations about the mean; and instantaneous quantities are denoted by a tilde. The x, y and z (x, r, θ) velocity components are given by variants of u, v and w, respectively. Vorticity component directions are denoted by their subscript, and δ is used to denote the boundary layer thickness, pipe radius or half-channel height.

In all cases, the starting point of the analysis is the mean differential statement of dynamics. For the channel, the appropriately simplified form of this equation is given by

$$\rho(\langle w\omega_y\rangle - \langle v\omega_z\rangle) = -\frac{\mathrm{d}P}{\mathrm{d}x} + \mu\frac{\mathrm{d}^2U}{\mathrm{d}y^2}, \tag{2.1}$$

where μ is the dynamic viscosity and ρ is the mass density. This equation indicates that the time-averaged effect of turbulent inertia (*TI*) on the left, see (2.4), is balanced by the driving mean pressure-gradient force (*PG*) and the opposing mean viscous force (*VF*) on the right.

For the pipe, the mean dynamical equation is given by

$$\rho(\langle w\omega_r\rangle - \langle v\omega_\theta\rangle) = -\frac{\mathrm{d}P}{\mathrm{d}x} + \frac{\mu}{r}\frac{\mathrm{d}}{\mathrm{d}r}\left(r\frac{\mathrm{d}U}{\mathrm{d}r}\right), \tag{2.2}$$

where the (u, v, w) velocity components are associated with an (x, r, θ) coordinate frame. Through the coordinate transformation, $y = \delta - r$, and use of the once-integrated form of (2.2), we obtain

$$u_\tau^2\left(1 - \frac{y}{\delta}\right) + \langle uv\rangle = \nu\frac{\mathrm{d}U}{\mathrm{d}y}. \tag{2.3}$$

Equation (2.2) takes on the same form as (2.1), i.e.

$$\frac{\mathrm{d}\langle uv\rangle}{\mathrm{d}y} = \langle w\omega_y\rangle - \langle v\omega_z\rangle = \frac{u_\tau^2}{\delta} + \nu\frac{\mathrm{d}^2U}{\mathrm{d}y^2}, \tag{2.4}$$

where we have employed $\nu = \mu/\rho$ and the boundary condition relating the pressure gradient to the wall shear stress, τ_w, or, equivalently, to the friction velocity, $u_\tau = \sqrt{\tau_w/\rho}$. As in the channel, the mean statement of dynamics for the pipe indicates that *TI* is balanced by the sum of *PG* and *VF*.

https://doi.org/10.1017/jfm.2012.626 Published online by Cambridge University Press

Similarly, application of the boundary layer approximations to the problem of flow over a flat plate yields

$$\rho\left(U\frac{\partial U}{\partial x}+V\frac{\partial U}{\partial y}+\langle w\omega_y\rangle-\langle v\omega_z\rangle\right)=\mu\frac{\partial^2 U}{\partial y^2}. \tag{2.5}$$

This equation indicates that the terms on the left, associated with the inertia of the mean flow (*MI*) and the time-averaged influence of turbulent inertia (*TI*), are balanced by the mean viscous force (*VF*) on the right. Distinct from convention, the mean effect of turbulent inertia in (2.4) and (2.5) is presented in its vorticity (non-conservative) form. This is useful for purposes of physical interpretation (see e.g. Eyink 2008; Klewicki 2010).

The mathematical developments are simplified by using

$$\langle w\omega_y\rangle-\langle v\omega_z\rangle=\frac{\mathrm{d}\langle uv\rangle}{\mathrm{d}y}=-\frac{\mathrm{d}T}{\mathrm{d}y} \tag{2.6}$$

in (2.4) and (2.5), where $T=-\langle uv\rangle$. Expression (2.6) is exactly satisfied in fully developed pipe and channel flows, and is satisfied to within the boundary layer approximation in the zero-pressure-gradient boundary layer (Tennekes & Lumley 1972; Klewicki 1989; Eyink 2008).

It is useful also to present (2.4) and (2.5) in their inner-normalized forms. Following convention, a superscript $+$ denotes normalization by the kinematic viscosity, ν, and the friction velocity, u_τ. The equation for pipes and channels becomes

$$-\frac{\mathrm{d}T^+}{\mathrm{d}y^+}=\epsilon^2+\frac{\mathrm{d}^2U^+}{\mathrm{d}y^{+2}}, \tag{2.7}$$

where $\epsilon^2=1/\delta^+$, and the boundary layer equation becomes

$$\left(U^+\frac{\partial U^+}{\partial x^+}+V^+\frac{\partial U^+}{\partial y^+}-\frac{\partial T^+}{\partial y^+}\right)=\frac{\partial^2 U^+}{\partial y^{+2}}. \tag{2.8}$$

2.1. *The four-layer structure*

Because there are only three operative dynamical effects in (2.7) or (2.8), in each case the ratio of any two exposes how the balance is realized. Given the high Reynolds-number magnitude ordering of terms in turbulent wall flows, this is best accomplished by examining the ratio of *VF* to *TI* (see e.g. Wei *et al.* 2005; Klewicki *et al.* 2007; Fife *et al.* 2009). Figure 1 displays a schematic representation of the ratio of the mean viscous force to the mean effect of turbulent inertia at a fixed Reynolds number beyond the transitional regime. For the channel and pipe this means that $\delta^+=\delta u_\tau/\nu$ is greater than $\sim$180 (Elsnab *et al.* 2011; Klewicki *et al.* 2012), while for the boundary layer $\delta^+\gtrsim 360$ (Klewicki *et al.* 2011).

The sketch of figure 1 effectively reflects the mean free-body diagram for the differential fluid elements at each position within the layer. A non-trivial balance can occur due to either two or three co-dominant terms. The balance for channels and pipes is attained according to a different ordering in four distinct layers as described in table 1.

Within the pipe or channel there is a well-defined region, of width $O(\nu/u_\tau)$, that abuts the wall and within which the mean viscous force and pressure-gradient force balance to leading order, attaining an exact balance right at the wall. This balance constitutes a boundary condition on the vorticity field that physically accounts for the

https://doi.org/10.1017/jfm.2012.626 Published online by Cambridge University Press

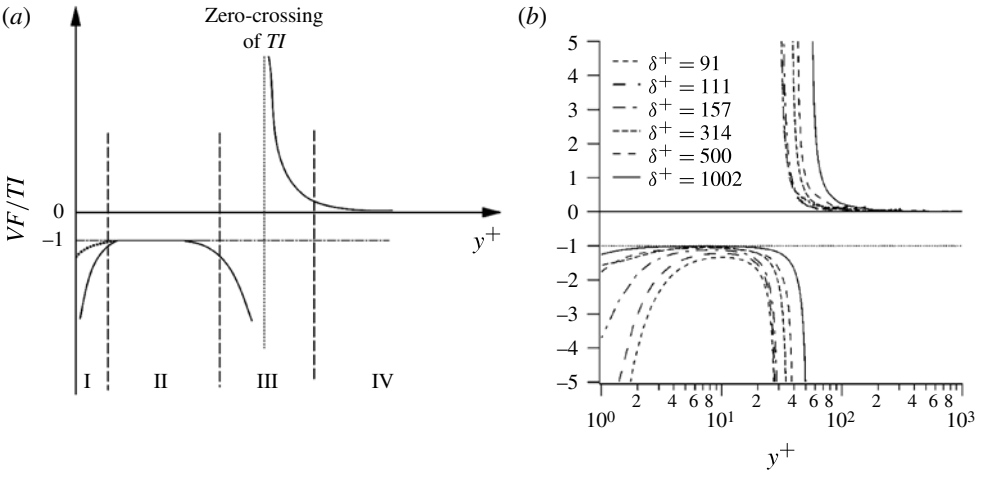


FIGURE 1. Ratio of the mean viscous force (VF) to mean effect of turbulent inertia (TI) in turbulent wall flows. (a) Sketch at fixed Reynolds number (dotted line in layer I distinguishes the boundary layers from pipe and channel flows); adapted from Wei *et al.* (2005). (b) Profiles from pipe flow DNS over a range of low δ^+; adapted from Klewicki *et al.* (2012).

Physical layer	Pipe and channel	Boundary layer
I	$\lvert PG\rvert \simeq \lvert VF\rvert \gg \lvert TI\rvert$	$\lvert MI\rvert \simeq \lvert VF\rvert \gg \lvert TI\rvert$
II	$\lvert VF\rvert \simeq \lvert TI\rvert \gg \lvert PG\rvert$	$\lvert VF\rvert \simeq \lvert TI\rvert \gg \lvert MI\rvert$
III	$\lvert PG\rvert \simeq \lvert VF\rvert \simeq \lvert TI\rvert$	$\lvert MI\rvert \simeq \lvert VF\rvert \simeq \lvert TI\rvert$
IV	$\lvert PG\rvert \simeq \lvert TI\rvert \gg \lvert VF\rvert$	$\lvert MI\rvert \simeq \lvert TI\rvert \gg \lvert VF\rvert$

TABLE 1. Magnitude ordering of the terms in the mean momentum equation on the layers depicted in figure 1. Note that, in the boundary layer, layer II may extend closer to the wall than in channel or pipe flow, as it does for Couette flow; see Wei *et al.* (2005), Wei, Fife & Klewicki (2007), Klewicki *et al.* (2011) and appendix A.

continuous flux of mean spanwise vorticity into the flow. Similarly, there is an equal and opposite annihilation of mean vorticity in pipes and channels that (presumably) occurs in the vicinity of the pipe or channel centreline. As described by Klewicki *et al.* (2012), however, the geometric differences between pipes and channels cause one to suspect that this annihilation process occurs differently in these two flows. In contrast, neither this process of mean vorticity annihilation nor the mean flux of vorticity into the flow at the wall are present in the zero-pressure-gradient boundary layer.

The structure of figure 1 is an outcome of the flow development through the transitional regime for each of the canonical flows considered (Elsnab *et al.* 2011; Klewicki *et al.* 2011, 2012). This structure arises due to the emergence of turbulent inertia. As explained in greater detail in appendix A, this structure is not only sustained, but becomes increasingly well defined, for all subsequent increases in δ^+. Owing to this, the associated scaling properties also become increasingly well defined as $\delta^+ \to \infty$. The theory described in § 3 derives from the properties admitted by the mean momentum equation as constrained by the magnitude ordering of terms associated with the structure of figure 1 (Fife *et al.* 2005*b*, 2009).

https://doi.org/10.1017/jfm.2012.626 Published online by Cambridge University Press

Physical layer	Δy increment (Δ_i)	ΔU increment ($\lvert\Gamma_i\rvert$)
I	$O(\nu/u_\tau)$ ($\lesssim 3$)	$O(u_\tau)$ ($\lesssim 3$)
II	$O(\sqrt{\nu\delta/u_\tau})$ ($\simeq 1.6$)	$O(U_\infty)$ ($\simeq 0.5$)
III	$O(\sqrt{\nu\delta/u_\tau})$ ($\simeq 1.0$)	$O(u_\tau)$ ($\simeq 1$)
IV	$O(\delta)$ ($\to 1$)	$O(U_\infty)$ ($\to 0.5$)

TABLE 2. Scaling behaviours of the layer thicknesses and velocity increments associated with the mean momentum equation (see figure 1). Note that the layer IV properties are asymptotically attained as $\delta^+ \to \infty$ (after Klewicki *et al.* 2007).

2.2. *Scaling properties of the four-layer structure*

The properties of the four-layer structure vary with Reynolds number. These behaviours derive from the rates at which the derivatives of U and T vary (decay) with increasing distance from the wall. As a consequence, both the widths and velocity increments across the four layers exhibit well-defined scaling behaviours. The scaling properties of the four-layer structure have been analytically determined and empirically verified, and are listed in table 2. Given the discussion above regarding layer I, its width is listed as being not greater than ~ 3 viscous units.

Layers II and III scale with the intermediate length, $\sqrt{\nu\delta/u_\tau}$. Using dimensional arguments, Bradshaw (1967) associated this length with the 'centre' of the pressure fluctuations in the boundary layer, while Long & Chen (1981) incorporated it within a broader (and somewhat speculative) theoretical description of turbulent flows. An associated observation made by Long & Chen (1981) and many other researchers (e.g. Afzal 1982; Sreenivasan & Sahay 1997; Wei *et al.* 2005) is that the wall-normal position of the maximum value of T^+, T_m^+, becomes fixed at $y/\sqrt{\nu\delta/u_\tau} \simeq 1.9$ as the Reynolds number becomes large. To the author's knowledge, Afzal was the first to identify the significance of this length within the context of the governing equations. He used the once-integrated momentum equation (2.3) for pipe flow to deduce the existence of an intermediate layer (see Afzal 1982, and references therein). Since then, Afzal and coworkers (see e.g. Afzal 2009) have used this length in a number of treatments that employ the overlap layer hypothesis of Izakson (1937) and Millikan (1939).

The present theory is distinct from these and other similar approaches, as it is not based on an overlap layer hypothesis, a similarity hypothesis, or any form of phenomenological model (e.g. Klewicki 2010). Instead, it relies solely upon the properties of the mean dynamical equation as constrained by the boundary conditions and the ordering of its terms in the four-layer regime. These analyses reveal that the intermediate length scale, $\sqrt{\nu\delta/u_\tau}$, arises because it constitutes an average property of an underlying layer width distribution, $W^+(y^+)$; see § 3.3 below. The analyses of Fife *et al.* (2005*a*) and Wei *et al.* (2007) for pipes and channels reveal that functions that scale with the mechanism of turbulent inertia should exhibit invariance when normalized by this length over a domain starting near $y \simeq y_m - \sqrt{\nu\delta/u_\tau}$, and extending outward to $y \simeq \delta$. This outer invariance is approached differently in boundary layers as $\delta^+ \to \infty$; see § 3.2 below. The $W^+(y^+)$ distribution is difficult to estimate accurately from experimental measurements. In this case, the intermediate length can be used as a surrogate to characterize certain statistical properties. When using direct numerical simulation (DNS) data, the $W^+(y^+)$ distribution can often be used directly. Both normalizations are thus useful for the purposes of data analysis.

https://doi.org/10.1017/jfm.2012.626 Published online by Cambridge University Press

The growth rates of the layer thicknesses can be found by differentiating the layer width entries in table 2 with respect to δ^+. Beginning with

$$\delta^+ = \Delta_I^+ + \Delta_{II}^+ + \Delta_{III}^+ + \Delta_{IV}^+, \tag{2.9}$$

we find that

$$\Delta_{IV}^+ \simeq \delta^+ - 2.6\sqrt{\delta^+} - 3.0, \tag{2.10}$$

and thus

$$\frac{\mathrm{d}\Delta_I^+}{\mathrm{d}\delta^+} = 0, \quad \frac{\mathrm{d}\Delta_{II}^+}{\mathrm{d}\delta^+} \simeq \frac{0.8}{\sqrt{\delta^+}}, \quad \frac{\mathrm{d}\Delta_{III}^+}{\mathrm{d}\delta^+} \simeq \frac{0.5}{\sqrt{\delta^+}}, \quad \frac{\mathrm{d}\Delta_{IV}^+}{\mathrm{d}\delta^+} \simeq 1 - \frac{1.3}{\sqrt{\delta^+}}. \tag{2.11}$$

These relations describe how scale separation effects are realized across the flow, and with increasing Reynolds number.

Increasing δ^+ is now considered, and for simplicity ν is held constant. In this case, the total circulation per unit length is given by $\Gamma_\infty = -U_\infty$ for the boundary layer, and $\Gamma_c = -U_c$ for pipes or channels. Thus, for fully developed flows, an increase in Reynolds number is always accompanied by an increase in $|\Gamma_c|$. In the boundary layer, however, δ^+ can increase at fixed Γ_∞ by simply allowing the flow to develop over a greater x distance. According to Reynolds-number similarity, the confinement of increasing total vorticity in a boundary layer of fixed δ^+ but increasing U_∞ (increasing $|\Gamma_\infty|$) is dynamically equivalent to the spreading of a fixed Γ_∞ over an increasing δ. This equivalence also has relevance to describing scale separation effects at different y locations within turbulent wall flows (see Morrill-Winter 2012).

Combining $|\Gamma_\infty^+| = U_\infty^+$ with the velocity increment scalings of table 2 identifies where, and at what rate, the increased circulation (per unit length) associated with an increase in U_∞^+ is apportioned. Specifically,

$$\Gamma_\infty = \int_0^\delta \Omega_z \,\mathrm{d}y = \Gamma_I + \Gamma_{II} + \Gamma_{III} + \Gamma_{IV}, \tag{2.12}$$

where $\Omega_z = -\mathrm{d}U/\mathrm{d}y$ (exactly in the pipe and channel, and to within Prandtl's approximations in the boundary layer), and

$$\frac{\mathrm{d}\Gamma_\infty^+}{\mathrm{d}\delta^+} = -\frac{\mathrm{d}U_\infty^+}{\mathrm{d}\delta^+}, \tag{2.13}$$

and also

$$\frac{\mathrm{d}\Gamma_I^+}{\mathrm{d}\delta^+} = \frac{\mathrm{d}\Gamma_{III}^+}{\mathrm{d}\delta^+} = 0, \quad \frac{\mathrm{d}\Gamma_{II}^+}{\mathrm{d}\delta^+} = \frac{\mathrm{d}\Gamma_{IV}^+}{\mathrm{d}\delta^+} \simeq 0.5\frac{\mathrm{d}\Gamma_\infty^+}{\mathrm{d}\delta^+}. \tag{2.14}$$

3. Mean flow theory

The four-layer structure and its attendant scaling behaviours constitute foundational elements of a mathematically cogent and mechanistically descriptive mean flow theory (Wei *et al.* 2005, 2007; Fife *et al.* 2005*a*,*b*, 2009; Metzger, Adams & Fife 2008; Klewicki *et al.* 2009, 2011, 2012). This subsection outlines and clarifies the elements of this theory most relevant to the present aims, and briefly describes some of the salient differences between channel, pipe and boundary layer flows.

3.1. *Elements of the channel and pipe flow analysis*

A number of the Reynolds-number scaling properties associated with the U and T profiles in the four-layer regime have been analytically determined and empirically

https://doi.org/10.1017/jfm.2012.626 Published online by Cambridge University Press

verified (Wei *et al.* 2005; Fife *et al.* 2005*a*, 2009; Klewicki *et al.* 2009). A central finding is that the equations of motion can be written in an invariant form on each of a continuous hierarchy of scaling layers, called the L_β hierarchy.

Each of the L_β layers on the hierarchy has a structure similar to layer III in figure 1. To show this, one begins with (2.7) and applies the transformation

$$T_\beta(y^+) = T^+(y^+) + \epsilon^2 y^+ - \beta y^+, \tag{3.1}$$

where on each layer the parameter β has a small positive and constant value. This yields the exact equation

$$\frac{\mathrm{d}^2 U^+}{\mathrm{d}y^{+2}} + \frac{\mathrm{d}T_\beta}{\mathrm{d}y^+} + \beta = 0. \tag{3.2}$$

Across each L_β layer the local mean dynamics undergoes a *balance breaking and exchange* of terms analogous to what occurs across layer III in figure 1. For each value of β, the T_β function attains a maximum value, $T_{\beta m}$, at a position $y_m^+(\beta)$ on the hierarchy, with $y_m^+(\beta)$ increasing as β decreases. As with layer III, the corresponding $y_m^+(\beta)$ is centrally located within each hierarchy layer, and thus on each L_β layer (as on layer III) all three terms in (3.2) are of the same order of magnitude. This motivates the need to rescale (3.2) such that all terms are formally $O(1)$ independent of β for all ϵ. Differential transformations of the form

$$\mathrm{d}y^+ = \beta^{-1/2}\,\mathrm{d}\hat{y}, \quad \mathrm{d}T^+ = \beta^{1/2}\,\mathrm{d}\hat{T} \quad \text{and} \quad \mathrm{d}U^+ = \mathrm{d}\hat{U} \tag{3.3}$$

are the simplest that accomplish this task. The invariant form

$$\frac{\mathrm{d}^2 U^+}{\mathrm{d}\hat{y}^2} + \frac{\mathrm{d}\hat{T}}{\mathrm{d}\hat{y}} + 1 = 0 \tag{3.4}$$

results, and is operative on every layer of the L_β hierarchy (Fife *et al.* 2009).

Figure 2 schematically depicts the hierarchy structure. The smallest member of the L_β hierarchy is situated in the inner part of layer II, and the largest extends well into layer IV. The layer widths vary with distance from the wall as determined by the parameter β (see (3.13) below), and, in doing so, span the scales of motion between those characterized by the inner and outer lengths, respectively. This property exposes the origin of the *distance from the wall* scaling that is often assumed in wall-flow analyses (Fife *et al.* 2005*a*,*b*).

Virtually all of the properties of the hierarchy stem from the fact that (2.1) admits the invariant form (3.4) on each L_β layer. This dynamical self-similarity is most succinctly expressed in terms of the scaled gradient of the mean effect of turbulent inertia. It states that the quantity

$$A(\beta) = -\frac{\mathrm{d}^2 \hat{T}_\beta}{\mathrm{d}\hat{y}^2}(0) = -\beta^{-3/2}\frac{\mathrm{d}^2 T^+}{\mathrm{d}y^{+2}} \tag{3.5}$$

becomes an $O(1)$ function on the L_β hierarchy (Fife *et al.* 2009). The $\hat{\cdot}$ in (3.5) indicates normalization using the characteristic length scale on each L_β layer, the subscript β refers to the transformed function (3.1) associated with each value of the parameter β, and the '0' refers to evaluation at the position of $\hat{T}_m(\beta)$ for each L_β. Essentially, (3.5) states that there is a region of concave-downward curvature in the $T^+ = -\langle uv\rangle^+$ profile for which (2.7) admits an exact self-similar form. At any finite δ^+, the dynamical self-similarity is approximate, and as $\delta^+ \to \infty$ the approximation

https://doi.org/10.1017/jfm.2012.626 Published online by Cambridge University Press

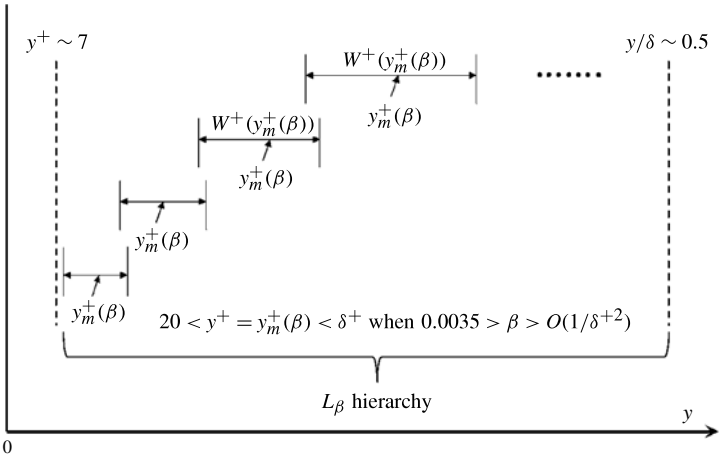


FIGURE 2. Schematic representation of the continuous hierarchy of scaling layers; the L_β hierarchy. On each member of the hierarchy, the governing dynamical equation admits an invariant form. The characteristic width of each layer is given by $W^+(y^+)$. For each value of β, the transformed function, T_m^β, is centrally located on its corresponding L_β layer.

improves. Further analyses suggest that these properties of $A(\beta)$ correlate with vorticity stretching in layer II, and the rate at which vorticity disperses via advective transport throughout layer IV (Morrill-Winter 2012).

Over an internal subdomain, $A(\beta)$ may attain exact or approximate constancy. Under either of these conditions, (3.5) provides an explicit closure, and thus allows direct integration of the mean momentum equation. These integrations yield a logarithmic mean velocity profile having the form

$$U^+ = \frac{4}{A^2}\ln(y^+ - C) + D, \tag{3.6}$$

where $A = A(\beta)$ and C and D are constants. Thus, the theory indicates that in a region of logarithmic dependence (exact or more generally approximate) the leading coefficient of (3.6) equals $4/A^2$ (exactly or approximately). Wall-flow data in the four-layer regime indicate that A most rapidly attains constancy on a subdomain that begins where the leading-order mean dynamics first becomes inertial (onset of layer IV), and ends interior to the wall-normal position of maximal length scale on the hierarchy (Wei *et al.* 2005; Fife *et al.* 2009; Klewicki *et al.* 2009).

Equation (3.6) differs from the classical logarithmic formula in two important ways: the leading coefficient in (3.6) has a direct analytical connection to the mechanism of turbulent inertia; and (3.6) has an offset, C. A number of recent studies either provide empirical evidence supporting the existence of an offset, or formally predict it. Analyses by Oberlack (2001) using Lie group theory show that, if the symmetries admitted by the Navier–Stokes equations are augmented with the symmetries associated with the velocity product equation, then the time-averaged equation for shear flow formally admits a logarithmic solution having the form of (3.6). This correspondence is not particularly surprising, since both the present theory and that by Oberlack (2001) are based upon determining the invariant forms admitted by the governing equations (Klewicki 2010). This is the rigorous basis for determining the existence of similarity solutions (Hansen 1964; Stephani 1989; Cantwell 2002).

https://doi.org/10.1017/jfm.2012.626 Published online by Cambridge University Press

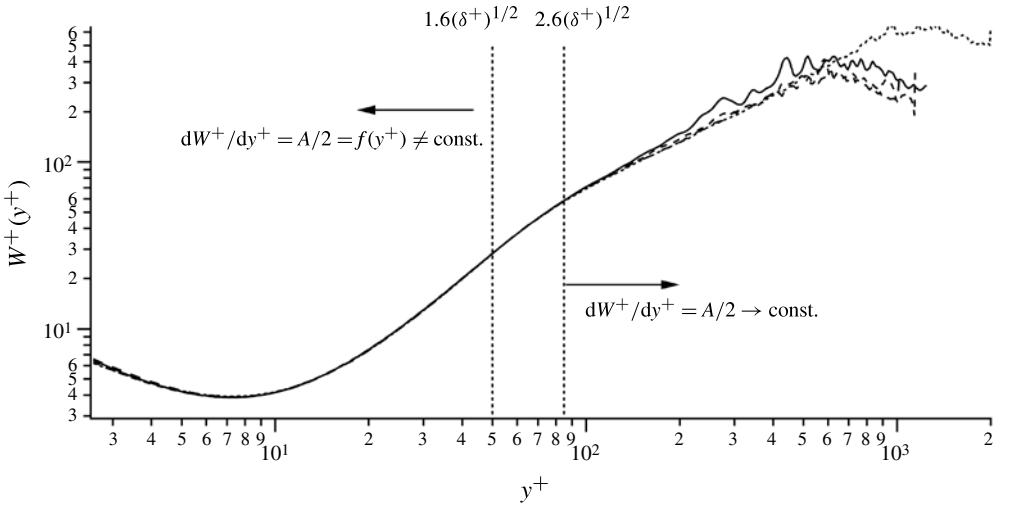


FIGURE 3. Characteristic width distribution of the L_β hierarchy versus y^+ for pipe, channel and boundary layer flows: - - - -, pipe flow DNS of Wu & Moin (2008) at $\delta^+ = 1142$; ——, boundary layer DNS of Schlatter & Orlu (2010) at $\delta^+ = 1245$; – – –, channel flow DNS of Abe, Kawamura & Matsuo (2004) at $\delta^+ = 1020$; ·····, channel flow DNS of Hoyas & Jimenez (2006) at $\delta^+ = 2004$. Vertical lines denoting the beginning and end of layer III are computed for $\delta^+ = 1000$.

For channels and pipes, perhaps the most comprehensive empirical documentation of the value for the offset is by Wosnik, Castillo & George (2000). Based upon an analysis of profiles covering $180 \lesssim \delta^+ \lesssim 530\,000$, they found that $C \simeq 8$. The present theory predicts that the value of the offset coincides with the start of the L_β hierarchy depicted in figure 2. Figures 3–5 indicate that this occurs near $y^+ = 7$, and thus this theoretical prediction is in accord with the observations of Wosnik *et al.* (2000). Other studies have found negative values for the offset. From an analysis of their Ekman boundary layer DNS, Spalart, Coleman & Johnstone (2008) found that an offset of $C = -7.5$ yielded the largest extent of logarithmic-like dependence. Within the context of the overlap layer hypothesis, Mizuno & Jimenez (2011) utilized curve fits in concert with a mixing length model and found best-fitting values for C equal to -8.5 and 3.8 for channels and boundary layers, respectively. Their analysis went up to $\delta^+ \simeq 8500$ in the boundary layer and $\delta^+ \simeq 4000$ in the channel. The offset appears in the formula of Mizuno & Jimenez (2011) owing to their use of a higher-order approximation. This is distinct from the overlap-layer-based arguments of Spalart *et al.* (2008) and Wosnik *et al.* (2000), which portray the offset as part of the leading-order equation. Based upon physical arguments, Spalart *et al.* (2008) indicate that the offset should be fixed, while the theory employed by Wosnik *et al.* (2000) indicates that this quantity could depend on δ^+.

3.2. *Elements of the boundary layer analysis*

The boundary layer analysis is analogous to that for the channel, but is complicated by an x dependence, and by the non-constancy of the mean advection profile in (2.8) over $0 \leqslant y \leqslant \delta$. The primary mathematical features that underlie Reynolds-number dependence are, however, retained.

https://doi.org/10.1017/jfm.2012.626 Published online by Cambridge University Press

For equilibrium boundary layer flows, (2.8) is well approximated by

$$\frac{\mathrm{d}^2U^+}{\mathrm{d}y^{+2}} + \frac{\mathrm{d}T^+}{\mathrm{d}y^+} + \epsilon^2 b(y^+, \epsilon) = 0, \tag{3.7}$$

where $\epsilon = \epsilon(x^+)$ and $b = b(y^+, \epsilon)$ (Metzger *et al.* 2008; Klewicki *et al.* 2011). The unknown $O(1)$ function b is constrained such that $\int_0^{\delta^+} b\,\mathrm{d}y^+ = O(\delta^+)$ for all ϵ. Given this, integration of (3.7) yields $\epsilon^{-2}(x^+) = O(\delta^+)$. Thus, the function b predominantly describes the shape of the mean advection profile, and ϵ describes its Reynolds-number variation.

Equation (3.7) is amenable to the methodology just described for channel and pipe flow. This equation admits an invariant form on each of a continuous hierarchy of internal scaling layers, and, as before, the position and width of each member of the L_β hierarchy is determined by the small parameter, β. The boundary layer case uses the transformation

$$T_\beta(y^+) = T^+(y^+) - T^*(\eta, \epsilon) - \beta y^+, \tag{3.8}$$

where $\eta = \epsilon^2 y^+ = O(y/\delta)$. In (3.8), $T^*(\eta, \epsilon)$ is the outer approximation to T^+,

$$T^* = \int_\eta^{\eta(\delta)} b(s, \epsilon)\,\mathrm{d}s, \tag{3.9}$$

where $\eta(\delta)$ denotes the value of $\eta = O(1)$ at $y = \delta$. Substitution of (3.8) into (3.7) yields

$$\frac{\mathrm{d}^2U^+}{\mathrm{d}y^{+2}} + \frac{\mathrm{d}T^+}{\mathrm{d}y^+} + \beta = 0, \tag{3.10}$$

which is of a form identical to (3.4). From here, the same set of differential transformations (3.3) yield the same invariant form of the differential force balance on each L_β layer.

While (3.10) is identical to (3.2), one should bear in mind that β in the boundary layer depends on an integral of the mean advection function, b, whose order-of-magnitude properties are known, but whose detailed features are unknown. Recall that in pipes or channels the pressure gradient is independent of y^+, and thus the outer approximation for T^+ can be expressed as an explicit function of y/δ. A net result of this is that, while the boundary layer $U^+(y^+)$ profile is expected to be increasingly well approximated by a logarithmic function as $\delta^+ \to \infty$, the variable nature of b leads one to doubt that an exactly logarithmic function is attained in the limit.

The boundary layer expression for $A(\beta)$ is also given by (3.5). As in pipes and channels, $A(\beta)$ is assured to remain $O(1)$ on the L_β hierarchy, and as $\delta^+ \to \infty A(\beta)$ is expected to increasingly approximate constancy on an interior domain of the hierarchy.

For the boundary layer, (3.5) implicitly includes the dependence of β on the mean advection profile. This is demonstrated by examining the expression that relates the inner-normalized derivative of TI to $A(\beta)$ (Metzger *et al.* 2008),

$$\frac{\mathrm{d}^2T^+(y_m^+(\beta))}{\mathrm{d}y^{+2}} = -A(\beta)\beta^{3/2} - \epsilon^2\frac{\mathrm{d}b(y_m^+(\beta))}{\mathrm{d}\beta}, \tag{3.11}$$

where, as before, $y_m^+(\beta)$ corresponds to $\hat{y} = 0$ for each β.

https://doi.org/10.1017/jfm.2012.626 Published online by Cambridge University Press

3.3. *The hierarchy length scale distribution, $W^+(y^+)$*

A primary attribute of the L_β hierarchy is its associated distribution, $W^+(y^+)$, which measures the inner-normalized width of each L_β layer as a function of y^+. Note that in previous publications W was used to denote the inner-normalized layer width distribution. Herein we use W^+, and thus W is the associated dimensional quantity. As described by Fife *et al.* (2005*b*), W^+ is the distribution of *natural* length scales that, when used to normalize (2.7), results in the invariant form (3.4) on each L_β layer. For all of the flows considered, the W^+ distribution is given by

$$W^+(y^+) = O(\beta^{-1/2}). \tag{3.12}$$

For pipes and channels the values of the parameter β can be evaluated using

$$\beta = \frac{\mathrm{d}T^+}{\mathrm{d}y^+} + \epsilon^2, \tag{3.13}$$

whereas for the boundary layer it involves evaluation of (3.9). For the purposes of computation, however, it is easier to use $\beta = -\mathrm{d}^2U^+/\mathrm{d}y^{+2}$.

The theory specifies that, through its connections to $A(\beta)$, the asymptotically linear behaviour of W^+ is (among other things) directly related to the leading coefficient of the logarithmic equation for the mean velocity (3.6). In all of the flows considered, $W^+(y^+)$ increasingly approaches a linear function on the hierarchy as $\delta^+ \to \infty$. Equation (3.12) is an order-of-magnitude statement. Once in the four-layer regime, however, the slope of W^+, $\mathrm{d}W^+/\mathrm{d}y^+$, begins to approximate a constant value (i.e. $A/2 \simeq$ const.) in a domain starting near the outer edge of layer III. Apparently, the constancy of the pressure-gradient function (possibly in combination with the simplest of boundary conditions among the three flows) causes the slope of $W^+(y^+)$ in channels to provide most rapidly a precise estimate for the asymptotic leading coefficient of the logarithmic profile equation, $4/A^2$. Klewicki *et al.* (2009) analysed the channel flow simulations of Hoyas & Jimenez (2006) and showed that in this flow the leading coefficient is estimated to be 0.39. This directly supports the analytical result that $\mathrm{d}W^+/\mathrm{d}y^+ = \sqrt{A^2/4} = A/2$ (Fife *et al.* 2005*a*). Existing evidence indicates that the pipe flow W^+ profile is very similar to that in the channel, but not necessarily exactly the same (Klewicki *et al.* 2012). In the boundary layer, W^+ rapidly becomes linear in the specified domain, but its slope (at low δ^+) is larger. Evidence provided herein indicates that this occurs due to the differences between the outer-region mean vorticity profile development in boundary layers versus channels and pipes. In all cases, however, the constancy of $\mathrm{d}W^+/\mathrm{d}y^+ = A/2$ beginning near $y/\sqrt{\nu\delta/u_\tau} = y^+/\sqrt{\delta^+} = 2.6$ indicates one kind of self-similar mean dynamical structure. For $y/\sqrt{\nu\delta/u_\tau} < 2.6$, existing evidence indicates that $W^+(y^+)$ approaches an invariant function of y^+ more slowly, indicating that the mean dynamics asymptotically adheres to a more complicated kind of self-similarity.

The scaling hierarchy upon which $W^+(y^+)$ is defined is estimated to have the lower edge of its smallest L_β layer begin near $y^+ = 7$, and the outer edge of its largest layer end near $y/\delta = 0.5$ (Fife *et al.* 2005*a*). As made apparent by (3.5), these positions occur near to where TI attains its positive and negative maximal values in the lower portion of layer II and middle of layer IV, respectively.

The features of $W^+(y^+)$ just described are exemplified in figure 3. This figure presents profiles of $W^+(y^+)$ from $\delta^+ \simeq 1000$ channel, pipe and boundary layer flows. To gain a sense of Reynolds-number variation, the channel flow profile of Hoyas & Jimenez (2006) at $\delta^+ = 2004$ is also presented. For a region near the wall, all

https://doi.org/10.1017/jfm.2012.626 Published online by Cambridge University Press

of these profiles convincingly follow a single curve. All of the profiles also attain their minimum values at $y^+ \simeq 7$, which is the position, y^+_{pi}, where $\mathrm{d}T^+/\mathrm{d}y^+$ attains a positive local maximum, and, equivalently, where T^+ passes through an inflection point, indicating a curvature change from concave-upward to concave-downward. The curves of figure 3 begin to exhibit approximately linear behaviour most convincingly at a position near $y^+ = 90$ ($\simeq 2.6\sqrt{\delta^+}$). Consistent with the theory, this linearity becomes more exact and extends over a greater y^+ range as δ^+ increases. This is seen by comparing the $\delta^+ = 1020$ and $\delta^+ = 2004$ channel flow profiles. The boundary layer W^+ profile at $\delta^+ = 1245$, while still approximately linear, has a noticeably larger slope than either the pipe or channel profiles – the latter two demonstrating much closer agreement. Klewicki *et al.* (2011) provide evidence that this behaviour has its origin in the transitional flow regime, and derives from both the shape and magnitude of the boundary layer mean advection profile changing with increasing δ^+. Conversely, the analogous pressure-gradient profile in pipes and channels has a fixed (constant) shape that only changes magnitude with δ^+.

The outer-region $W^+(y^+)$ profiles exhibit a peak value. The position of this peak marks the end of the L_β hierarchy (Fife *et al.* 2009; Klewicki *et al.* 2009). As predicted by the theory, the position of W^+_{max} occurs near $y/\delta = 0.5$ (Fife *et al.* 2005*a*). For channels and pipes, existing evidence indicates that, once in the four-layer regime, the position of W^+_{max} is between $y/\delta = 0.45$ and 0.55 (Klewicki *et al.* 2009, 2012). Similarly, available DNS data (all at low δ^+) indicate that this position resides between $0.48 \lesssim y/\delta \lesssim 0.55$ in the boundary layer. Owing to the constancy of the pressure-gradient function, the position of the peak value of $|\mathrm{d}T^+/\mathrm{d}y^+|$ in the outer region, y^+_{po}, exactly corresponds to the position of W^+_{max} in pipes and channels. In the boundary layer, the mean advection profile varies, and available data indicate that y^+_{po} occurs somewhat farther from the wall $0.5 \lesssim y_{po}/\delta \lesssim 0.7$ – at least at low δ^+ (Klewicki *et al.* 2011).

When interpreted as a force, the mean mechanism of turbulent inertia behaves like a momentum source for $y^+ < y^+_m$, and like a momentum sink for $y^+ > y^+_m$ (Wei *et al.* 2005; Klewicki *et al.* 2007). Recall that y^+_m is the position where T^+ attains its maximum, T^+_m, or, equivalently, where TI crosses zero (see figure 1). Owing to

$$\int_0^{\delta^+} \frac{\mathrm{d}T^+}{\mathrm{d}y^+}\,\mathrm{d}y^+ = 0, \tag{3.14}$$

the net source and sink contributions sum to zero at any given δ^+. For the present purposes, it is useful to demonstrate this by plotting the profiles of $\mathrm{d}T^+/\mathrm{d}y^+$ pre-multiplied by $W^+(y^+)$. (Note that profiles having nearly the same shape are also generated by plotting $y^+\,\mathrm{d}T^+/\mathrm{d}y^+$, but in that case the peaks in the resulting function correspond less closely to the actual peaks in $\mathrm{d}T^+/\mathrm{d}y^+$.) Because $W^+(y^+)$ is the *natural* length scale distribution for this profile, the weighted source and sink contributions exhibit an approximately symmetrical shape between the positive and negative maxima. This behaviour is exemplified by the profiles of $W^+\,\mathrm{d}T^+/\mathrm{d}y^+$ in figure 4.

All of the $W^+\,\mathrm{d}T^+/\mathrm{d}y^+$ profiles of figure 4 convincingly fall on the same curve for a region beginning in layer I and extending into the lower part of layer II, out to $y^+ \simeq 40$. Interior to y^+_m, however, the boundary layer profile diverges from the channel and pipe profiles. Consistent with the flatter T^+ profile near its peak, the boundary layer $W^+\,\mathrm{d}T^+/\mathrm{d}y^+$ profile exhibits a shallower trajectory through zero. The channel and pipe flow profiles are nearly the same, although small differences in the

https://doi.org/10.1017/jfm.2012.626 Published online by Cambridge University Press

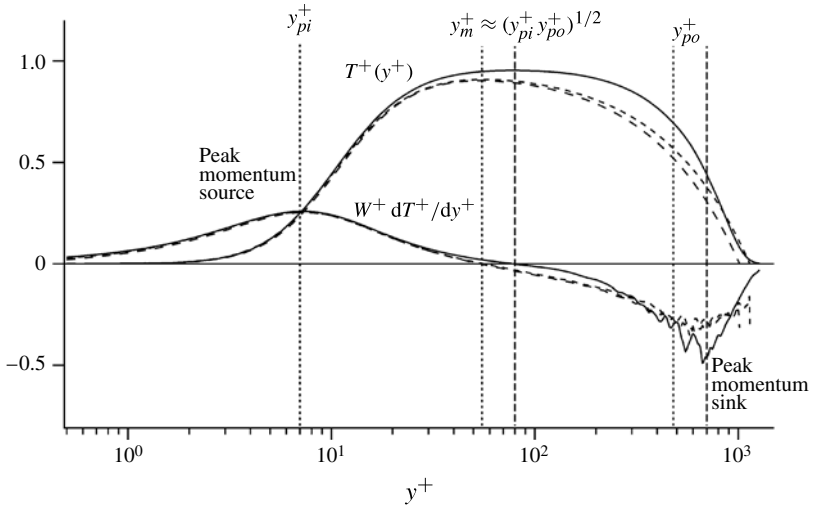


FIGURE 4. Inner-normalized distributions of T^+ and $W^+ \mathrm{d}T^+/\mathrm{d}y^+$ versus y^+ for pipe, channel and boundary layer flows. Line styles are the same as in figure 3. Vertical dotted lines are associated with the pipe and channel data, and the vertical dashed lines pertain to the boundary layer profiles. Note that pre-multiplication of $\mathrm{d}T^+/\mathrm{d}y^+$ by W^+ reveals the mean source–sink balance associated with the mechanism of turbulent inertia.

outer T^+ profiles are observed. In layer IV, the boundary layer $W^+ \mathrm{d}T^+/\mathrm{d}y^+$ profile crosses the channel and pipe profiles, and attains a greater negative peak value. It is surmised that this larger peak is associated with the different outer boundary condition on $\mathrm{d}T^+/\mathrm{d}y^+$ in the boundary layer. In the pipe and channel, the value of $\mathrm{d}T^+/\mathrm{d}y^+$ approaches ϵ^2 $(=1/\delta^+)$ as $y \to \delta$, whereas in the boundary layer $\mathrm{d}T^+/\mathrm{d}y^+$ smoothly goes to zero as $y^+ \to \infty$. Thus, the higher peaked $W^+ \mathrm{d}T^+/\mathrm{d}y^+$ profile in the boundary layer is the combined result of this different boundary condition and the constraint imposed by (3.14). These observations indicate that, relative to pipes and channels, the velocity vorticity correlations in (2.6) behave quite differently in the outer region of boundary layers. Physically, this difference is likely to be associated with the imposed outer-region annihilation of Ω_z in pipes and channels, and its absence in boundary layers. As indicated in figure 4, the value of y^+_m is well approximated by $\sqrt{y^+_{pi} y^+_{po}}$. This stems from the fact that layer III (centred about y^+_m) comprises the average (or central) layer on the L_β hierarchy (e.g. Klewicki *et al.* 2007, 2011).

4. Similarity solutions

The preceding exposition of the theory and its ramifications establish a useful context for clarifying the nature and veracity of the self-similar structure exposed by the analysis. To do this, we first return to the condition for dynamic similarity (3.5), and more fully describe the properties of $A(\beta)$ and $W^+(y^+)$.

Figure 5 shows profiles of $A(\beta)$ across the lower portion of the L_β hierarchy at $\delta^+ \simeq 1000$ for boundary layer, pipe and channel flows, and also for the channel at $\delta^+ = 640$ and 2004. At $\delta^+ = 1000$ the region shown in figure 5 encompasses all but the lowest portion of layer II, layer III and the lower part of layer IV. The quantity $A(\beta)$ becomes positive at $y^+ = y^+_{pi} \simeq 7$; and $W^+(y^+)$ most rapidly exhibits a constant slope beginning in the region where layer III transitions into layer IV (Klewicki *et al.*

https://doi.org/10.1017/jfm.2012.626 Published online by Cambridge University Press

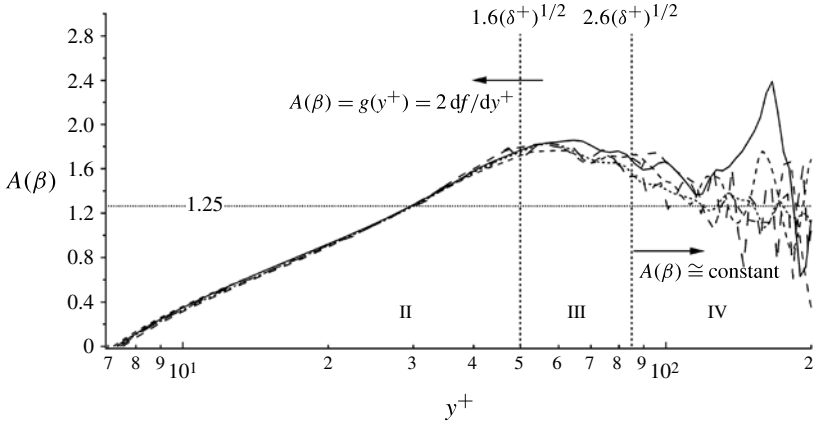


FIGURE 5. Profiles of $A(\beta)$ from pipe, channel and boundary layer flows on the inner portion of the L_β hierarchy: - - - -, pipe flow DNS of Wu & Moin (2008) at $\delta^+ = 1142$; ——, boundary layer DNS of Schlatter & Orlu (2010) at $\delta^+ = 1034$; — — —, channel flow DNS of Abe *et al.* (2004) at $\delta^+ = 640$; – – –, channel flow DNS of Abe *et al.* (2004) at $\delta^+ = 1020$; · · · · · ·, channel flow DNS of Hoyas & Jimenez (2006) at $\delta^+ = 2004$. Note that, if, for $y^+ \lesssim y_m^+$, $A(\beta) = g(y^+)$ and $W^+(y^+) = f(y^+)$, then $g(y^+) = 2\,df/dy^+$; see figure 3.

2009). This also corresponds to the region where A begins to approximate constancy most rapidly (Fife *et al.* 2005*b*, 2009). The quantity $A(\beta)$ is a considerably more sensitive statistic to compute in layer IV than W^+. This is demonstrated in figure 5 by the erratic behaviour of A beginning in layer III and with increasing amplitude in layer IV. The reason for this sensitivity is primarily attributable to the uncertainties associated with differentiating discrete data, as computations verify that the estimation of A from dW^+/dy^+ (as opposed to fitting a line to the W^+ profile) yields the same result as from (3.5).

Despite this erratic behaviour, existing data confirm that, with increasing δ^+, A increasingly approaches constancy over an increasing y^+ domain. This is exemplified in figure 6, which shows the dA/dy^+ profile derived from the $\delta^+ = 2004$ simulation of Hoyas & Jimenez (2006). The indicated linear curve fit over $90 \lesssim y^+ \lesssim 450$ is given by $dA/dy^+ = -0.0011 + (2.2 \times 10^{-7})y^+$. (Owing to the increasingly higher-amplitude oscillations about zero, curve fits to higher y^+ become increasingly sensitive to their endpoint.) The inset reveals that dA/dy^+ reaches a maximum value near the outer edge of layer I. Consistent with the theory, dA/dy^+ rapidly decreases to a magnitude much less than unity near the start of the hierarchy. The abrupt change in the slope of the inset curve near $y^+ = 40$ correlates with the results of Morrill-Winter (2012) associated with the changing size of the motions bearing $\tilde{\omega}_z$.

Equation (3.5) is found by solving for the transformations that render (2.7) invariant on each layer of the L_β hierarchy. Effectively, (3.5) indicates that, when appropriately scaled by a function of its magnitude, the wall-normal rate of change of the mean mechanism of turbulent inertia (normalized flux of turbulent force) increasingly becomes an invariant $O(1)$ positive function over an interior domain. The length scale (layer width) distribution, W^+, reflects the spatial stretching commensurate with this property of TI adhering to the invariant form (3.5). On the inner part of the L_β hierarchy, $A(\beta)$ is well approximated by an invariant, but non-constant, positive function. Similarly, W^+ is well approximated by an invariant but nonlinear function

https://doi.org/10.1017/jfm.2012.626 Published online by Cambridge University Press

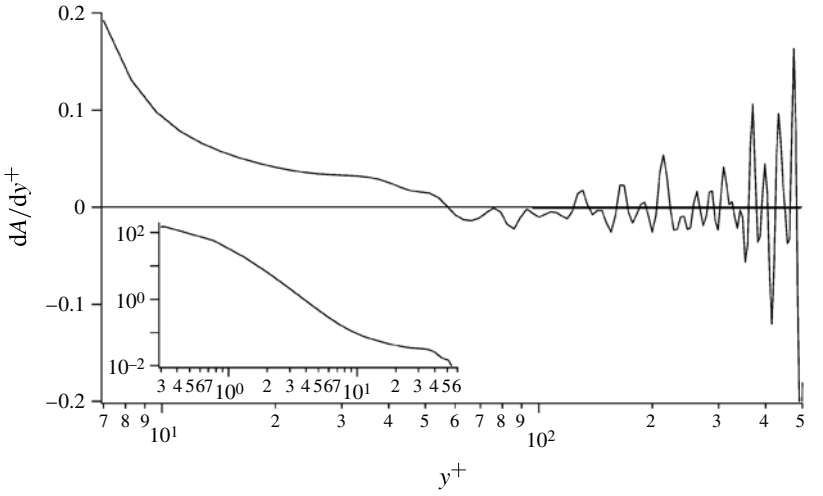


FIGURE 6. Profile of the derivative of $A(\beta)$ from the channel flow DNS of Hoyas & Jimenez (2006) at $\delta^+ = 2004$. Curve fit (full line) for $90 \lesssim y^+ \lesssim 450$ is given by $\mathrm{d}A/\mathrm{d}y^+ = -0.0011 + (2.2 \times 10^{-7})y^+$.

of y^+. On an adjacent part of this domain, $A(\beta)$ approaches constancy, while W^+ approaches a linear function of y^+.

As discussed relative to (3.6), the underlying dynamical self-similarity allows the mean momentum equation to be directly integrated for the case in which A equals a constant (approximately or exactly). The capacity to directly integrate the mean momentum equation implies its analytical closure. Specifically, it has long been known that similarity properties (symmetries), if admitted by a differential equation, can lead to a net reduction in the number of relevant variables (Morgan 1952). In the present case, the derived similarity condition (3.5) constitutes a reduction in variables that directly relates a derivative of U^+ to a derivative of T^+, and thus analytically closes the mean dynamical equation (Klewicki *et al.* 2009). As now described, (3.5) also allows one to cast the mean momentum equation for wall flows into a form that is more readily recognized as a genuine similarity solution.

The equation for the mean vorticity is found by taking the curl of the mean momentum equation. For pipe and channel flow, this equation is exactly given by

$$0 = \frac{\mathrm{d}^2\Omega_z^+}{\mathrm{d}y^{+2}} + \frac{\mathrm{d}^2T^+}{\mathrm{d}y^{+2}}, \tag{4.1}$$

while it holds to within the boundary layer approximation for the flow over a flat plate. Combining (4.1) and (3.5) yields

$$\frac{\mathrm{d}^2\Omega_z^+}{\mathrm{d}y^{+2}} + A(\beta)\left[\frac{\mathrm{d}\Omega_z^+}{\mathrm{d}y^+}\right]^{3/2} = 0. \tag{4.2}$$

The theory indicates that $A(\beta)$ equals twice the slope of the $W^+(y^+)$ profile over the hierarchy. With increasing δ^+ this slope increasingly approximates constancy on the inertial domain starting near $y^+ = 2.6\sqrt{\delta^+}$, and ending interior to $y/\delta = 0.5$. Klewicki *et al.* (2009) show that, for the $\delta^+ = 2004$ simulation of Hoyas & Jimenez (2006) (whose $W^+(y^+)$ profile is shown in figure 3), $A(\beta)$ is well approximated by a constant

https://doi.org/10.1017/jfm.2012.626 Published online by Cambridge University Press

value of 1.25. Given this, (4.2), (2.7) and (2.3), we obtain that

$$\frac{\mathrm{d}\Omega_z^+}{\mathrm{d}y^+} - \frac{\mathrm{d}T^+}{\mathrm{d}y^+} - \epsilon^2 = 0, \tag{4.3}$$

$$\Omega_z^+ + 1 = T^+ + \epsilon^2 y^+ \tag{4.4}$$

and

$$\frac{\mathrm{d}U^+}{\mathrm{d}y^+} = -\Omega_z^+ \tag{4.5}$$

constitute a closed system of ordinary differential equations for U^+, Ω_z^+, T^+ and their derivatives. This system is analytically closed through use of the relations specified by the theory, and with the analysis (2.7) only relying upon the magnitude ordering of terms indicated by figure 1.

As is common for such problems (e.g. the flat-plate laminar boundary layer), at least some of the boundary conditions for the system of equations are not *a priori* known. Furthermore, the present system of equations gains the indicated invariance properties on an internal domain, while similarity solutions in the laminar regime generically adhere to the same invariance condition throughout the entire flow. The internal domain is indicated by the theory to reside interior to W_{min} and W_{max}. The mean dynamics on the domain of interest is inertially dominated, and thus begins near the outer edge of layer III ($y^+ \simeq 2.6\sqrt{\delta^+}$), and ends interior to the position of W_{max} ($y/\delta \simeq 0.5$). The starting values for the numerical integration can be estimated to within about $\pm 5\,\%$ using a combination of theory and observations. Test calculations reveal, however, that the computed solution is sensitive to the accuracy of the starting values, and increasingly so with increasing δ^+. For the present purposes, it is thus more useful to simply select the starting values from a DNS. Since the similarity properties become increasingly apparent as the Reynolds number gets large, we use the highest-Reynolds-number DNS available: the channel flow simulation of Hoyas & Jimenez (2006) at $\delta^+ = 2004$. The computation requires U^+, Ω_z^+ and $\mathrm{d}\Omega_z^+/\mathrm{d}y^+$ at $y^+ = 2.6\sqrt{\delta^+} \simeq 115$. At $y^+ = 115.103$, the DNS solution gives $U^+ = 16.7675$, $\Omega_z^+ = -0.0209$ and $\mathrm{d}\Omega_z^+/\mathrm{d}y^+ = 0.000\,16$. These values were used to start a standard ordinary differential equation solver, which took a couple of seconds to run. In accordance with the theory, the integration was carried out to $y/\delta \simeq 0.5$.

Figure 7 shows that the profiles determined from the similarity solution exhibit excellent agreement with those derived from the DNS. In addition, comparison of the $\mathrm{d}\Omega_z^+/\mathrm{d}y^+$ and $\mathrm{d}^2\Omega_z^+/\mathrm{d}y^{+2}$ profiles reveals that the DNS solution begins to develop numerical uncertainties as y^+ becomes large, or, equivalently, as these functions become small. Even here, however, the similarity solution faithfully tracks the profiles found by time averaging the direct numerical solution of the full Navier–Stokes equation.

Use of the logarithmic vertical axis in figure 7 allows all of the functions appearing in (4.2)–(4.5) to be plotted on a single figure. This logarithmic axis also makes it difficult to scrutinize the accuracy of the U^+ and T^+ profiles, as these functions vary relatively slowly with y^+. Figure 8 shows the profiles of U^+ and T^+ over the same y^+ range, but plotted on semi-logarithmic axes. This graph reveals that the T^+ profile from the DNS and similarity solution are indistinguishable (everywhere agreeing to within 1 part in 1000), while the U^+ profile starts to exhibit a small but discernible difference from the DNS near $y^+ = 600$. This degradation of the similarity solution is anticipated from the theory, since boundary influences are expected to cause

https://doi.org/10.1017/jfm.2012.626 Published online by Cambridge University Press

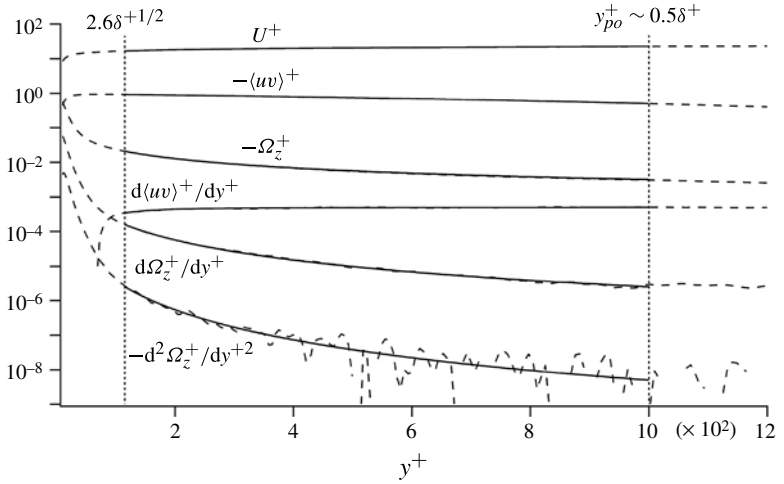


FIGURE 7. Comparison of the inner-normalized profiles of U^+, Ω_z^+, $\mathrm{d}\Omega_z^+/\mathrm{d}y^+$, T^+, $\mathrm{d}^2\Omega_z^+/\mathrm{d}y^{+2}$ and $\mathrm{d}T^+/\mathrm{d}y^+$ on the domain $2.6\sqrt{\delta^+} \leqslant y^+ \leqslant \delta^+/2$ as determined from the $\delta^+ = 2004$ channel flow DNS of Hoyas & Jimenez (2006) (– – –) and by integrating the analytically closed system of ordinary differential equations (4.2)–(4.5) with starting values determined from the DNS (——).

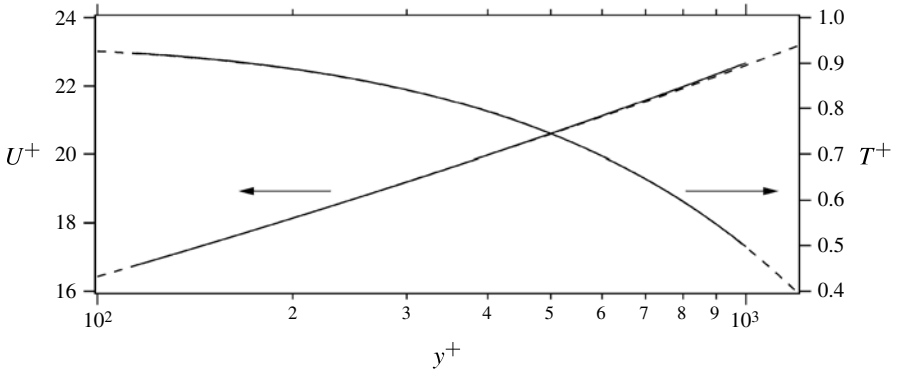


FIGURE 8. Expanded view of the U^+ and $T^+ = -\langle uv\rangle^+$ profiles from figure 7.

imperfections in the self-similar dynamics at the periphery of the L_β hierarchy (see e.g. Fife *et al.* 2009). The maximum deviation from the DNS U^+ profile (at $y^+ = 1000$) is $\sim$0.35 %, while for $y^+ \lesssim 600$ the deviation is everywhere less than 0.1 %.

Close examination reveals that the U^+ profiles of figure 8 are not exactly straight lines, and thus are not exactly logarithmic. As described in § 3, at any finite δ^+, the U^+ profile is only approximately logarithmic, with the accuracy of the approximation improving as δ^+ increases. The present solution inherently reflects these behaviours, as they are indicative of the emerging self-similarity as δ^+ increases. At any finite δ^+, the similarity solution is, for example, neither a logarithmic nor a power function; rather, it is most accurately described as a solution to (2.4). The boundary layer similarity solution exhibits behaviours much like those in figure 7, with its accuracy to within the approximations of the formulation summarized in § 3.2. For the sake of

https://doi.org/10.1017/jfm.2012.626 Published online by Cambridge University Press

completeness, examples of the similarity solutions for the pipe and boundary layer are given in appendix B.

5. Discussion and conclusions

The present theoretical framework is self-contained within the boundary value problem that describes the mean dynamics, as constrained by the magnitude ordering of terms graphically depicted by the four-layer structure of figure 1. This structure has been confirmed to emerge through the transitional regime (Elsnab *et al.* 2011; Klewicki *et al.* 2011, 2012); see e.g. figure 1(*b*). All of the mathematical and mechanistic descriptions are understood relative to the behaviours of the terms in the appropriate equation of mean dynamics. There is no reliance on notions that relate $T^+ = -\langle uv\rangle^+$ to a shear-stress-like function, as, for example, (2.1) clearly reveals that this is not the case. Similarly, their is no reliance on the existence (or non-existence) of the von Kármán constant, κ, which arises from the use of approaches that are not well founded in the mean dynamical equation.

Evidence of the self-similarities predicted by the theory are apparent in other recent analyses. For example, by using an iterative curve-fitting procedure, Mizuno & Jimenez (2011) demonstrate that for the $\delta^+ = 2004$ flow of figure 7 their modified mixing length model exhibits its optimal behaviour over a domain that extends from $\sim 100 \lesssim y^+ \lesssim 1100$. The present theoretical prediction indicates that the onset of the self-similarity associated with $A(\beta) \simeq$ const. begins near $y^+/\sqrt{\delta^+} = 2.6$ and ends near $y/\delta = 0.5$, or, equivalently, between $y^+ \simeq 116$ and $y^+ \simeq 1000$ at this Reynolds number. Mizuno & Jimenez (2011) also note that their lower bound can, to a good approximation, be extended downwards to about $y^+ = 70$. This is consistent with the findings of Klewicki *et al.* (2009) that the self-similarity predicted to appear first near $y^+/\sqrt{\delta^+} = 2.6$ is approximately satisfied interior to this point with increasing δ^+.

These observations are clarified by noting that on the L_β hierarchy the wall-normal coordinate stretching associated with self-similar behaviour is given by the function, ϕ, where

$$\frac{\mathrm{d}W}{\mathrm{d}y} = \frac{A(\beta)}{2} = \phi^{-1}. \tag{5.1}$$

The function ϕ is literally the rate at which the distance from the wall varies relative to the rate at which the mean size of the inertial turbulent motions varies. Conceptually, W is reminiscent of the mixing length (Fife *et al.* 2005*a*, 2009). This is most apparent when one considers von Kármán's representation (von Kármán 1930)

$$\ell_{mix} = \kappa \frac{\partial U/\partial y}{\partial^2 U/\partial y^2}. \tag{5.2}$$

Equation (5.2) is an intuited *similarity hypothesis*. From its construction, it is apparent that von Kármán sought to exploit this hypothesized self-similarity to close the mean momentum equation, i.e. effectively construct a similarity solution. The present approach accomplishes this by formally determining the coordinate stretching, ϕ, that yields an invariant form of the mean dynamical equation. Note that similar to (5.2), $A(\beta)$ is also expressed as a ratio of velocity derivative functions, e.g. (4.2); see also Klewicki *et al.* (2009) for equivalent alternative expressions for $A(\beta)$.

Empirical support for the theory described in § 3 is exemplified in figures 3–8. In combination, the theory and observations support the following assertions. For $y^+_{pi} \lesssim y^+ \lesssim 2.6\sqrt{\delta^+}$, dynamical similarity is manifest by an $A(\beta)$ (or ϕ) that is an

https://doi.org/10.1017/jfm.2012.626 Published online by Cambridge University Press

Flow	δ^+	$A(\beta)$	Integration domain	Starting values: U^+, Ω_z^+, $\mathrm{d}\Omega_z^+/\mathrm{d}y^+$
Channel	2004	1.25	$115.103 \leqslant y^+ \leqslant 1000$	16.768, −0.0209, 0.000 160
Pipe	1142	1.29	$88.524 \leqslant y^+ \leqslant 570$	16.118, −0.0272, 0.000 265
Boundary layer	1245	1.60	$91.152 \leqslant y^+ \leqslant 623$	16.149, −0.0253, 0.000 246

TABLE 3. Parameters employed in the channel, pipe and boundary layer integrations.

asymptotically invariant, $O(1)$, but non-constant, function of y^+. Regarding this, the results of figure 5 provide evidence of a weak Reynolds-number dependence between $40 \lesssim y^+ \lesssim 2.6\sqrt{\delta^+}$. For $2.6\sqrt{\delta^+} \lesssim y^+ \lesssim y_{po}^+$, $A(\beta)$ approximates an $O(1)$ constant, with the accuracy of the approximation improving as δ^+ increases. On this domain the coordinate stretching is also approximately constant, i.e. $\phi = \phi_c$. The analytical description of ϕ on the subdomain of the L_β hierarchy interior to $y^+/\sqrt{\delta^+} \simeq 2.6$ is the subject of on-going research.

The relative simplicity of the *outer* ($\phi = \phi_c$) similarity underlies the closure of the mean dynamical equation found by using (4.2). While ϕ approximates a constant on this domain, the entries of table 3 reveal that, at low δ^+, ϕ_c is not the same constant for the different canonical wall flows. (Note that the theory indicates that a region of approximately constant ϕ will yield a region of logarithmic-like behaviour.) Studies of transitional and nascent four-layer regime flows provide evidence that, in the pipe, and especially the boundary layer, ϕ_c becomes invariant with Reynolds number more slowly than in the channel (Elsnab *et al.* 2011; Klewicki *et al.* 2011, 2012). For the channel, the value of ϕ_c at $\delta^+ = 2004$ is 1.6, which corresponds to a von Kármán constant (coefficient), κ, of 0.39 (Klewicki *et al.* 2009). Recent high-δ^+ evidence from pipes and boundary layers suggests that κ asymptotes to a value of 0.39, and that this slope is attained starting near the outer edge of layer III (Marusic *et al.* 2013). Taken together, these findings suggest that, at sufficiently high Reynolds number, each of the canonical flows approach the same self-similar state on the $\phi = \phi_c$ subdomain, but that self-similar mean dynamics is well approximated on the hierarchy (at a given δ^+) significantly before this high-δ^+ condition is attained. Evidence of this assertion is given by the veracity of the boundary layer similarity solution (figure 10), even though $\phi_c \simeq 1.25$, and thus differs significantly from the high-δ^+ value of 1.6. These findings suggest that the notion of a universal κ is subsumed within the broader range of self-similar phenomena embodied in the coordinate stretching function, ϕ. Specifically, the totality of results support that κ is associated with the inertial domain asymptotic limit of ϕ, i.e. the high-δ^+ value of ϕ_c on the inertial domain bounded by $2.6\sqrt{\delta^+} \lesssim y^+ \lesssim 0.5\delta^+$.

The solutions of figures 7–10 reflect the similarities admitted by the relevant form of the mean momentum equation. Comparisons of $U^+(y^+)$ and $T^+(y^+)$ profiles (and their derivative profiles) from different experiments implicitly rely on the uniqueness of these equations. This motivates some brief comment on the potential equivalences between the present and other approaches. Two prevalent approaches have been examined in some detail. No connections have yet been found between the present approach and those that employ the assumption of an overlap layer (e.g. Mellor 1972; Afzal 1982; Wosnik *et al.* 2000; Monkewitz, Chauhan & Nagib 2008). Current indications suggest that no such connections are likely to exist (Fife *et al.* 2005*b*, 2009). Conversely, the solution properties on the $\phi = \phi_c$ portion of the

https://doi.org/10.1017/jfm.2012.626 Published online by Cambridge University Press

hierarchy are well aligned with descriptions based upon Townsend's *attached eddy hypothesis* (e.g. Perry & Chong 1982; Perry & Marusic 1995).

Acknowledgements

This work was partially supported by the U.S. Office of Naval Research (grant monitor R. Joslin) and the Australian Research Council. The researchers who made their DNS data sets available via the internet are gratefully acknowledged. The author expresses his continuing gratitude to Professor P. Fife for sharing his mathematical and physical insights.

Appendix A. On the four-layer ordering of terms

Essentially every theoretical approach that seeks to describe the statistical behaviours of wall turbulence relies on some level of empiricism, an *a priori* hypothesis, or other non-rigorous assumptions. The theory of Fife and coworkers (Fife *et al.* 2005*b*, 2009) employed herein uses measurements at the outset of the analysis to verify that the magnitude orderings of the terms found through analysis of the relevant forms of the mean momentum equation are indeed the actual magnitude orderings. Once these orderings are established, all of the remaining results from the theory reflect properties that are formally admitted by the relevant boundary value problem, i.e. found through analysis of the governing mean dynamical equation and its boundary conditions.

The four layers of figure 1 are described in § 2 as characterizing the asymptotic structure of turbulent wall flows. Specifically, the assertion is made that, once within the four-layer regime, the flow never enters a regime that is described by a different magnitude ordering of terms. Implications of this are that the scaling properties given in table 2 and as reflected in the similarity solution of figure 7 become more accurate as $\delta^+ \to \infty$. The following describes why this assertion is believed to be valid.

While there are a number of ways to approach this issue, the most straightforward is first to recognize that it is unambiguously known that the four-layer structure exists at low Reynolds number for each of the three canonical wall flows (Elsnab *et al.* 2011; Klewicki *et al.* 2011, 2012). The relevant question then pertains to what might cause this structure to change as $\delta^+ \to \infty$. In this regard, it is important to reiterate that, given the ordering of terms reflected by the four-layer structure, the layer widths and velocity increments are (in an order-of-magnitude sense) determinable through analysis of the governing mean equation alone (Fife *et al.* 2005*a*, 2009). The discussion below considers each layer individually.

Layer I. For pipe and channel flows, evaluation of the inner-normalized mean momentum equation at the wall yields

$$0 = \frac{1}{\delta^+} + \frac{\mathrm{d}^2 U^+}{\mathrm{d}y^{+2}}, \tag{A 1}$$

which indicates that the mean viscous force is always balanced by the mean pressure gradient at the wall. Relative to figure 1 (and disallowing discontinuous mean functions), this result indicates that, for all δ^+, the ratio of *VF* to *TI* becomes very large and negative as the wall is approached. Consideration of a Taylor series about $y = 0$ indicates that there will always be a neighbourhood of $y = 0$ where the *VF* and *PG* terms are of the same order of magnitude. Note that the magnitude of the balance expressed by (A 1) decreases like $1/\delta^+$, which is identically the rate at which ν/u_τ decreases relative to δ. This reasoning is recognizable as essentially that used to

https://doi.org/10.1017/jfm.2012.626 Published online by Cambridge University Press

deduce the existence of the viscous sublayer, and thus the thickness of layer I is also $O(\nu/u_\tau)$.

For the boundary layer, all of the terms in the mean momentum equation are zero at the wall, and thus the thickness of layer I depends upon the rates at which these terms approach zero as $y \to 0$. Existing evidence is inconclusive, but this leaves open the possibility that, in the boundary layer (and perhaps depending on δ^+), layer II may extend all the way to the wall. This is true for Couette flow at all δ^+, and Wei *et al.* (2007) examined this case in some detail. They found no apparent consequences relative to the other layer properties, and little disagreement with our current understanding of viscous sublayer dynamics.

Layer II. Note first that layer II exists at currently accessible δ^+. That is, all reliable evidence indicates that there is a region near the wall where the leading-order balance in the mean dynamical equation is between the *VF* and *TI* terms. We thus consider what must occur in either the channel or pipe for this local leading-order balance to change. The physical inadmissibility of a single leading-order term leads to the only possibility being that the *PG* term regains importance, and perhaps eventually swaps leading order with another term. Such a process, however, requires that, over some Reynolds-number range, the inner-normalized *VF* and *TI* terms in this part of the flow simultaneously decrease at a rate faster than $1/\delta^+$. For the boundary layer, the argument is identical, except, owing to the approximation of (3.7), the *VF* and *TI* terms would have to decrease simultaneously at a rate faster than $1/\delta^+$ multiplied by the $O(1)$ function, b.

Layer IV. Layer IV also unambiguously exists, as all relevant data indicate that there is a region away from the wall in which the leading-order balance involves the *PG* and *TI* terms in the channel or pipe. The behaviour of the *PG* term is exactly known as a function of Reynolds number. Thus, the only way for this balance to change is for the *VF* term to increase relative to the *TI* term in the outer region over some δ^+ range. Again, for the boundary layer, the argument is identical to within the $O(1)$ function, b.

Layer III. Given the existence of layers II and IV, the balance of all three terms in the relevant mean momentum equation must occur in a layer III between layers II and IV. This information and the mean momentum equation are sufficient to show analytically that the outer boundaries of layers II and III scale with $\sqrt{\nu\delta/u_\tau}$, and with this follow all of the other scaling behaviours as, for example, indicated in table 2 (Wei *et al.* 2005; Fife *et al.* 2005*a*,*b*, 2009).

The above considerations lead to the conclusion that, in the absence of additional forces or a change in boundary conditions, the four-layer structure and its order-of-magnitude scaling behaviours exist as described for all δ^+ beyond the transitional regime.

Appendix B. Similarity solutions for the pipe and boundary layer

Figures 7 and 8 show that the analytical closure derived by Fife *et al.* (2009) results in time-averaged profiles that accurately reproduce the findings from the channel DNS of Hoyas & Jimenez (2006) at $\delta^+ = 2004$. Figures 9 and 10 provide similar comparisons for pipe and boundary layer flow. For these we use the fully developed pipe flow DNS of Wu & Moin (2008) at $\delta^+ = 1142$, and the spatially developing boundary layer DNS of Schlatter & Orlu (2010) at $\delta^+ = 1245$. Note that, in both of these cases, the Reynolds number is significantly smaller than in the channel DNS. Given this, the theory indicates that the underlying self-similar structure will not be as well developed, but that the agreement between the data and the similarity solution

https://doi.org/10.1017/jfm.2012.626 Published online by Cambridge University Press

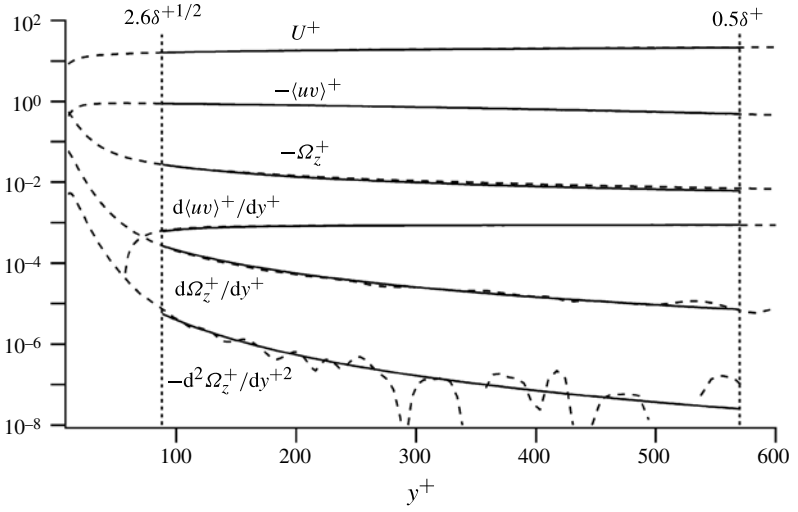


FIGURE 9. Comparison of the inner-normalized profiles of U^+, Ω_z^+, $\mathrm{d}\Omega_z^+/\mathrm{d}y^+$, T^+, $\mathrm{d}^2\Omega_z^+/\mathrm{d}y^{+2}$ and $\mathrm{d}T^+/\mathrm{d}y^+$ on the domain $2.6\sqrt{\delta^+} \leqslant y^+ \leqslant \delta^+/2$ as determined from the $\delta^+ = 1142$ pipe flow DNS of Wu & Moin (2008) (– – –) and by integrating the system of ordinary differential equations (4.2)–(4.5) with starting values determined from the DNS (——).

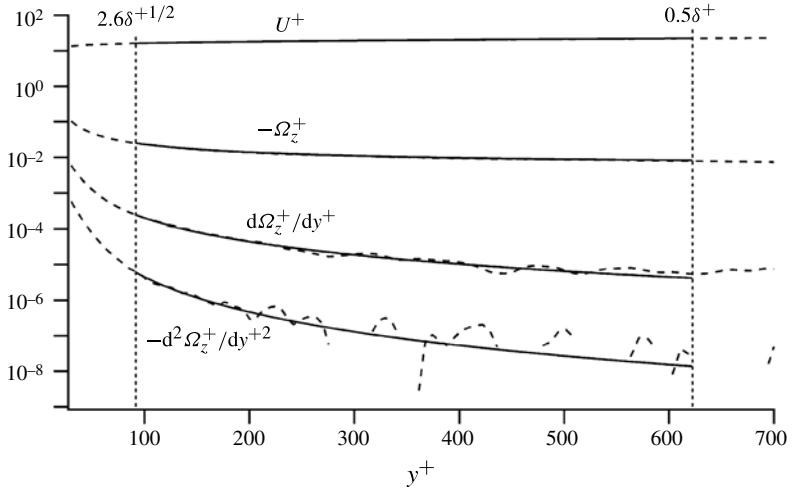


FIGURE 10. Comparison of the inner-normalized profiles of U^+, Ω_z^+, $\mathrm{d}\Omega_z^+/\mathrm{d}y^+$ and $\mathrm{d}^2\Omega_z^+/\mathrm{d}y^{2+}$ on the domain $2.6\sqrt{\delta^+} \leqslant y^+ \leqslant \delta^+/2$ as determined from the $\delta^+ = 1245$ boundary layer DNS of Schlatter & Orlu (2010) (– – –) and by integrating the ordinary differential equation (4.2) with starting values determined from the DNS (——).

should improve with increasing Reynolds number. This is exemplified by the boundary layer U^+ solution in figure 10. The maximum deviation of this profile from the DNS solution is ∼0.45 % (at $y/\delta \simeq 0.5$), as compared to the maximum deviation of ∼0.35 % exhibited by the channel flow solution of figure 7.

https://doi.org/10.1017/jfm.2012.626 Published online by Cambridge University Press

As in the case of the channel, we employ (4.2), with the understanding that in the boundary layer the hierarchy structure is influenced by a mean advection profile that varies with distance from the wall and Reynolds number. This influence is reflected in (3.11), which shows that the second derivative of T^+ depends on both $A(\beta)$ and the derivative of the advection function, b, with respect to β. A primary implication of this is that, while (4.2) and (4.1) can still be used to solve for the mean velocity and its derivatives (to within the boundary layer approximation), the contributions of T and b to $A(\beta)$ in (3.11) cannot be readily segregated, and thus one cannot directly integrate to solve for T and its derivatives. Since the equations for the pipe and channel are identical, the exact expressions for $\mathrm{d}T^+/\mathrm{d}y^+$ and T^+, (4.3) and (4.4), respectively, may be directly employed, since $\epsilon^2 = 1/\delta^+$ is a known constant.

Use of (4.2) requires that $A(\beta)$ be estimated. In each case, the most accurate way to do this is to evaluate the slope of the $W^+(y^+)$ profile starting at $y^+ \simeq 2.6\sqrt{\delta^+}$ (outer edge of layer III) and extending to $y/\delta \simeq 0.5$ (upper edge of the L_β hierarchy) (see Klewicki *et al.* 2009). This is the subdomain of the hierarchy where the leading-order contributions to the mean dynamics are inertial. It is also where $\phi = \phi_c$. The portion of this subdomain closest to $y^+ \simeq 2.6\sqrt{\delta^+}$ is best for empirically determining the slope of $W^+(y^+)$, as this is where the profile shows the least scatter, and is not near the edge of the hierarchy.

The $W^+(y^+)$ profiles for the three flows under consideration are given in figure 3. These profiles exhibit small but discernible differences in their slope over the domain of interest. Curve fits of the channel and pipe flow data yield values of $A = 1.25$ and 1.29, respectively Klewicki *et al.* (2009, 2012). A curve fit of the boundary layer W^+ profile yields $A = 1.60$. As described by Klewicki *et al.* (2012), the reasons for these differences are connected to the development of the outer-region vorticity field as influenced by the boundary conditions and the presence or absence of mean vorticity annihilation. A summary of the starting values for the channel, pipe and boundary layer integrations is given in table 3.

REFERENCES

ABE, H, KAWAMURA, H. & MATSUO, Y. 2004 Surface heat-flux fluctuations in a turbulent channel flow up to $Re_\tau = 1020$ with $Pr = 0.025$ and 0.71. *Intl J. Heat Fluid Flow* **25**, 404–419.

AFZAL, N. 1982 Fully developed turbulent flow in a pipe: an intermediate layer. *Ing.-Arch.* **52**, 355–377.

AFZAL, N. 2009 Analysis of instantaneous turbulent velocity vector and temperature profiles in transitional rough channel flow. *J. Heat Transfer* **131**, 064503.

BRADSHAW, P. 1967 'Inactive' motion and pressure fluctuations in turbulent boundary layers. *J. Fluid Mech.* **30**, 241–258.

CANTWELL, B. J. 2002 *Introduction to Symmetry Analysis*. Cambridge University Press.

ELSNAB, J., KLEWICKI, J., MAYNES, D. & AMEEL, T. 2011 Mean dynamics of transitional channel flow. *J. Fluid Mech.* **678**, 451–481.

EYINK, G. 2008 Turbulent flow in pipes and channels as cross-stream 'inverse cascades' of vorticity. *Phys. Fluids* **20**, 125101.

FIFE, P., KLEWICKI, J., MCMURTRY, P. & WEI, T. 2005*a* Stress gradient balance layers and scale hierarchies in wall-bounded turbulence. *J. Fluid Mech.* **532**, 165–189.

FIFE, P., KLEWICKI, J., MCMURTRY, P. & WEI, T. 2005*b* Multiscaling in the presence of indeterminacy: wall-induced turbulence. *Multiscale Model. Simul.* **4**, 936–959.

FIFE, P., KLEWICKI, J. & WEI, T. 2009 Time averaging in turbulence settings may reveal an infinite hierarchy of length scales. *J. Discrete Continuous Dyn. Syst.* **24**, 781–807.

HANSEN, A. 1964 *Similarity Analysis of Boundary Value Problems in Engineering*. Prentice-Hall.

https://doi.org/10.1017/jfm.2012.626 Published online by Cambridge University Press

HOYAS, S. & JIMENEZ, J. 2006 Scaling the velocity fluctuations in turbulent channels up to $Re_\tau = 2003$. *Phys. Fluids* **18**, 011702.

IZAKSON, A. 1937 On the formula for the velocity distribution near walls. *Tech. Phys. USSR IV* **2**, 155–162.

VON KÁRMÁN, T. 1930 Mechanische Ahnlichkeit und Turbulenz. *Nachr. Ges. Wiss. Gottingen, Math-Phys. Klasse* 155–162.

KLEWICKI, J. C. 1989 Velocity–vorticity correlations related to the gradients of the Reynolds stress in parallel turbulent wall flows. *Phys. Fluids* A **1**, 1285–1289.

KLEWICKI, J. 2010 Reynolds number dependence, scaling, and dynamics of turbulent boundary layers. *J. Fluids Engng* **132**, 094001.

KLEWICKI, J., CHIN, C., BLACKBURN, H., OOI, A. & MARUSIC, I. 2012 Emergence of the four layer dynamical regime in turbulent pipe flow. *Phys. Fluids* **24**, 045107.

KLEWICKI, J., EBNER, R. & WU, X. 2011 Mean dynamics of transitional boundary-layer flow. *J. Fluid Mech.* **682**, 617–651.

KLEWICKI, J., FIFE, P. & WEI, T. 2009 On the logarithmic mean profile. *J. Fluid Mech.* **638**, 73–93.

KLEWICKI, J., FIFE, P., WEI, T. & MCMURTRY, P. 2007 A physical model of the turbulent boundary layer consonant with mean momentum balance structure. *Phil. Trans. R. Soc.* A **365**, 823–839.

LAADHARI, F. 2011 An apparent symmetry property of the mean velocity gradient in turbulent Poiseuille flows and its implications. *Phys. Fluids* **23**, 101705.

LONG, R. R. & CHEN, T.-C. 1981 Experimental evidence for the existence of the mesolayer in turbulent systems. *J. Fluid Mech.* **105**, 19–59.

MARUSIC, I., MONTY, J., HULTMARK, M. & SMITS, A. 2013 On the logarithmic region in wall turbulence. *J. Fluid Mech.* **716**, R3.

MELLOR, G. L. 1972 The large Reynolds number, asymptotic theory of turbulent boundary layers. *Intl J. Engng Sci.* **10**, 851–873.

METZGER, M., ADAMS, P. & FIFE, P. 2008 Mean momentum balance in moderately favourable pressure gradient turbulent boundary layers. *J. Fluid Mech.* **617**, 107–140.

MILLIKAN, C. B. 1939 A critical discussion of turbulent flows in channels and circular tubes. In *Proceedings of Fifth International Congress of Applied Mechanics*, pp. 386–392. Wiley.

MIZUNO, Y. & JIMENEZ, J. 2011 Mean velocity and length scales in the overlap region of wall-bounded turbulent flows. *Phys. Fluids* **23**, 085112.

MONKEWITZ, P., CHAUHAN, K. & NAGIB, H. 2008 Comparison of mean flow similarity laws in zero pressure gradient turbulent boundary layers. *Phys. Fluids* **20**, 105102.

MORGAN, A. J. A. 1952 The reduction by one of the number of independent variables in some systems of partial differential equations. *Q. J. Math. Oxford* **3**, 250–259.

MORRILL-WINTER, C. 2012 Scale separation effects on mechanisms of wall turbulence. MS thesis, University of New Hampshire, Durham, NH, USA.

OBERLACK, M. 2001 Unified approach for symmetries in plane parallel shear flows. *J. Fluid Mech.* **427**, 299–328.

PERRY, A. & CHONG, M. 1982 On the mechanism of wall turbulence. *J. Fluid Mech.* **119**, 173–217.

PERRY, A. & MARUSIC, I. 1995 A wall-wake model for the turbulence structure of boundary layers. Part 1. Extension of the attached eddy hypothesis. *J. Fluid Mech.* **298**, 361–388.

SCHLATTER, P. & ORLU, R. 2010 Assessment of direct numerical simulation data of turbulent boundary layers. *J. Fluid Mech.* **659**, 116–126.

SPALART, P. R., COLEMAN, G. N. & JOHNSTONE, R. 2008 Direct numerical simulation of the Ekman layer: a step in Reynolds number, and cautious support for a log law with a shifted origin. *Phys. Fluids* **20**, 101507.

SREENIVASAN, K. R. & SAHAY, A. 1997 The persistence of viscous effects in the overlap region, and the mean velocity in turbulent pipe and channel flows. In *Self-Sustaining Mechanisms of Wall Turbulence* (ed. R. Panton), pp. 253–272. Computational Mechanics Publications.

STEPHANI, H. 1989 *Differential Equations: Their Solution Using Symmetries*. Cambridge University Press.

https://doi.org/10.1017/jfm.2012.626 Published online by Cambridge University Press

TENNEKES, H. & LUMLEY, J. 1972 *A First Course in Turbulence*. MIT Press.

WEI, T., FIFE, P. & KLEWICKI, J. 2007 On scaling the mean momentum balance and its solutions in turbulent Couette–Poiseuille flow. *J. Fluid Mech.* **573**, 371–398.

WEI, T., FIFE, P., KLEWICKI, J. & MCMURTRY, P. 2005 Properties of the mean momentum balance in turbulent boundary layer, pipe and channel flows. *J. Fluid Mech.* **522**, 303–327.

WOSNIK, M., CASTILLO, L. & GEORGE, W. K. 2000 A theory for turbulent pipe and channel flows. *J. Fluid Mech.* **421**, 115–145.

WU, X. & MOIN, P. 2008 A direct numerical simulation study on the mean velocity characteristics in turbulent pipe flow. *J. Fluid Mech.* **608**, 81–112.

https://doi.org/10.1017/jfm.2012.626 Published online by Cambridge University Press